Imaging Sustained Dissipative Patterns in the Metabolism of Individual Living Cells

Howard R. Petty,* Randall G. Worth, and Andrei L. Kindzelskii
Department of Biological Sciences, Wayne State University, Detroit, Michigan 48202
(Received 28 July 1999)

Theoretical studies have predicted spatiotemporal organization of cell metabolism. Using a rapidly gated CCD camera, we demonstrate for the first time sustained traveling waves of NAD(P)H autofluorescence and protons in individual morphologically polarized living cells. Chemical concentration fronts moved in the direction of cell orientation, thus correlating dissipative structures with cell shape.

PACS numbers: 87.17.–d, 87.16.Qp, 87.18.Pj, 87.64.–t

Spatiotemporal patterns are found in numerous physical, chemical, and biological settings [1]. When far from equilibrium, chemical systems can become unstable and spontaneously form spatiotemporal patterns [1,2]. One mechanism of chemical pattern formation involves the coupling of reaction and diffusion processes. Turing [3] first recognized the role of reaction-diffusion processes in generating stable chemical patterns and their possible role in embryogenesis. Turing structures are possible only under stringent conditions and have recently been observed in physico-chemical systems [4,5]. Nevertheless, other spatiotemporal patterns, such as propagating chemical waves, are possible [6]. Traveling chemical waves have been reported [7–9]. Although theoretical work has predicted spatial glycolytic patterns in cells [10–15], they have not been observed. However, they have been found in macroscopic cell extracts [16–19]. We test the hypothesis that dissipative metabolic structures occur in living cells. To observe dissipative structures, we imaged microscopically NAD(P)H autofluorescence or the emission of a proton-sensitive dye using a gated intensified charge-coupled device (ICCD) camera. We report nicotinamide adenine dinucleotide (phosphate) [NAD(P)H] and proton waves traveling parallel to the long axis of elongated cells that confirm dramatically prior theoretical predictions and extend spatiotemporal patterning to single cells.

Several judicious choices were made in experimental design. Since polarized neutrophils are ~ 20 μm in length, they approximate the minimal critical length for pattern formation ($l \sim 1$ to 100 μm) [10–15]. These cells spread on surfaces thereby thinning their cytoplasm; this minimizes out-of-focus fluorescence and the confounding influences of wave motion in the third dimension. Furthermore, glycolysis is particularly important for neutrophils [20]. Hence, the contribution of mitochondria to cell metabolism is less than that for other cell types. We took advantage of the fact that exposure of cells to PMA (phorbol myristate acetate) triples the amplitude of NAD(P)H oscillations (e.g., [21]), which increases the relative contrast in micrographs. Moreover, leukocyte activities create a high energy demand and hence greater metabolic flux. Previous studies of yeast extracts have shown NADH waves traveling at 5 μm/sec [16]. Assuming a similar velocity in cells, image acquisition times must be <40 msec to prevent blurring in comparison to the Rayleigh distance of $\simeq 0.2$ μm. However, as the detector is pulsed for shorter times, image quality suffers from shorter integration periods.

An axiovert fluorescence microscope with a quartz condenser, quartz objectives, a mercury lamp, and a stage maintained at 37° C (Zeiss Inc., New York, NY) was employed. For NAD(P)H imaging, cells were illuminated at 365 nm and fluorescence emission was collected using a 400 nm long-pass dichroic mirror and a 400 nm long-pass filter (Omega Optical, Brattleboro, VT). The pH sensitive probe 5- (and 6-) carboxy SNARF-1, acetoxymethyl ester, acetate (SNARF-1) (Molecular Probes, Eugene, OR) was detected using a $485/22$ nm excitation filter, a 510 nm long-pass dichroic mirror, and a $530/30$ nm emission filter. To minimize the number of optical components, the microscope's bottom port was fiber-optically coupled to the input side of an Acton-150 (Acton Instruments, Acton, MA) imaging spectrophotometer. The exit side was connected to a liquid nitrogen cooled intensifier (Gen-II) (~ -20 °C) attached to a Peltier-cooled I-MAX-512 camera (~ -20 °C) (Princeton Instruments Inc., Trenton, NJ). Image acquisition was controlled by a high-speed Princeton ST-133 interface and a Stanford Research Systems (Sunnyvale, CA) DG-535 delay gate generator. The imaging spectrophotometer's mirror was replaced by a ruled grating (300 gr/mm) for spectroscopy.

An imaging spectrophotometer was used to obtain autofluorescence emission spectra. Neutrophils were isolated as described [22]. The autofluorescence of reduced pyridine nucleotides (NADH and NADPH) is an established method to monitor the metabolic state of living tissues [23]. Figure 1 (thick line) shows an autofluorescence emission spectrum from a living cell, with an emission maximum at 460 nm. This emission peak corresponds to that of purified NADPH [24]. To rigorously link autofluorescence with cell metabolism, we measured the emission spectrum in the presence of the metabolic inhibitors 2-deoxy-D-glucose (100 mM) and sodium azide (3%) for 30 min at 37 °C. In the presence of inhibitors, $\sim 95\%$ of the autofluorescence

 0031-9007/00/84(12)/2754(4)$15.00

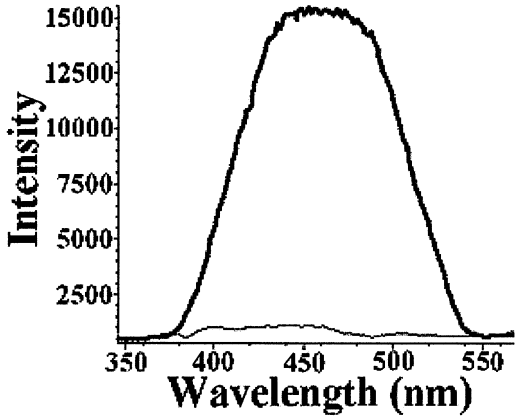

FIG. 1. Fluorescence emission spectra of single cells. A representative spectrum from an untreated cell is shown (thick line). The addition of 2-deoxy-*D*-glucose and sodium azide results in a ~95% reduction in signal (thin line).

intensity disappears (Fig. 1); this was not associated with cell rupture since plasma membranes remained intact as judged by trypan blue exclusion [22]. Furthermore, NAD(P)H emission linearly increases with NAD(P)H concentration [24]. Therefore, emission in this region is an excellent measure of metabolic activity.

Spontaneously polarized neutrophils were studied. Preliminary experiments were conducted to qualitatively assess imaging parameters; acceptable image quality was achieved using ≅10 msec acquisition times. Figure 2(A) shows a series of high speed (10 msec) NAD(P)H autofluorescence images of a PMA-primed (10 μm PMA for 15 min at 37 °C) cell. These micrographs illustrate the spatial patterns associated with neutrophils. Autofluorescent stripes move in the direction of cell orientation from the uropod → cell body → lamellipodium. The direction of stripe movement was inferred from Fig. 2(A) and from intervening photographic frames (not shown). Intracellular NAD(P)H emission patterns have not previously been observed [24]. This is accounted for by the integration time of the detector; longer acquisition times simply "average" the images to spatial homogeneity [Fig. 2(B)]. The spatially varying fluorescence emission was confirmed by selecting small pixel arrays at the uropod, cell body, and lamellipodium and then plotting the intensity of each region as a function of time [Fig. 2(C)]. This quantitatively confirmed the local time-varying intensity. It is possible that these patterns might be accounted for by a time-varying excitation pattern. To control for this factor, fluorescent latex beads (Polysciences Inc., Warrington, PA) were also studied. These experiments showed that the bead's intensity remained roughly constant [Fig. 2(C)] whereas that of the cells varied. Furthermore, changes in cell thickness cannot account for changing spatial patterns since the uropod, whose thickness is constant, oscillates through light and dark stages. Hence, self-organized spatial concentration patterns are formed in cells.

Several additional properties of NAD(P)H traveling waves can be noted. The stripe width is ≅3 to 4 μm. The light-dark repeat patterns are twice this distance. The

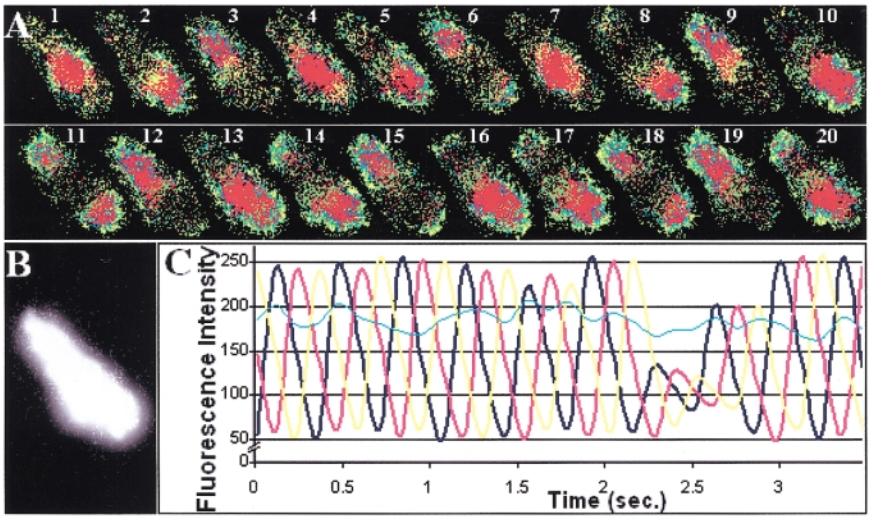

FIG. 2 (color). Visualization of traveling NAD(P)H waves in a polarized neutrophil. (A) Time sequence of 20 autofluorescence images of a PMA-activated neutrophil. The lamellipodium is oriented toward the lower right hand corner of each frame. Each image was collected for 10 msec with a 90 msec interval between micrographs. From all of the images collected for this cell, only every fifth image is shown here for clarity. To improve computer acquisition times, 125 × 165 pixel arrays were employed. The NAD(P)H concentration varies spatially; fluorescent stripes propagate from the uropod to lamellipodium. Pseudocolor images are shown (red = bright, black = dark). Images were collected at a central plane of focus. The total time covered by these images is 10 sec (×840). The images are representative of those obtained on nine independent experiments. (B) A micrograph of the same cell acquired over a 10 sec period (×920). (C) Quantitation of wave motion. The fluorescence intensity of a small pixel array was recorded as a function of time for three cytoplasmic regions (red = uropod, yellow = cell center, dark blue = lamellipodium, and light blue = bead). In addition to these spatial waves, global temporal oscillations of 20 sec have also been reported [21,22].

observed stripe size is consistent with calculations [15] showing that pattern elements must be >1 μm to overcome diffusional mixing. Wave velocity is estimated at ~ 10 μm/sec [Figs. 2(A) and 2(C)]. To exclude the possibility that the waves were traveling at a higher velocity, four intermediate frames were taken between each of the frames shown in Fig. 2(A). These data reveal incremental positions of the wave (data not shown), suggesting that higher velocities are not present. Interestingly, metabolic wave velocity in single cells is similar to that found for cell extracts (e.g., [16]), although at a far smaller scale. Although we have consistently obtained striped patterns in polarized cells, we have not observed such patterns in spherical cells. Thus, the formation of metabolic patterns correlates with morphological polarization.

To provide another line of evidence supporting the formation of metabolic dissipative structures, intracellular pH was studied. Protons are generated during glycolysis and the breakdown of $\mathrm{NAD(P)H} \rightarrow \mathrm{NAD(P)}^{+} + 2$ electrons $+ \mathrm{H}^{+}$. Cells were labeled with SNARF-1 at 50 ng/ml for 50 min at 37°, washed to remove unbound label, and transferred to microscope slides. Figure 3 shows a series of high speed SNARF-1 images of a PMA-primed cell. As anticipated, fluorescent stripes were again visualized using 10 msec CCD gating. The features of pH-associated fluorescence stripes recapitulated those of NAD(P)H. Thus, polarized cells are characterized by both NAD(P)H and pH patterns.

Living cells are open thermodynamic systems far from equilibrium. Some of the matter or energy absorbed from the environment can be used to create spatiotemporal order. Temporal chemical oscillations, a type of dissipative structure, have been described for various molecules [6]. NAD(P)H oscillations, which arise from glycolytic feedback control [23], have been described for neutrophils [21,22]. Dissipative structures can also involve spatial self-organization. To our knowledge, Figs. 2 and 3 present the first observations of spatial metabolite concentration patterns in living cells. Previous studies have predicted metabolic waves in cells [10–15]; our work confirms their existence. Studies [11,12] have predicted that the minimal cell size required for pattern formation is ~ 100 μm. This is about a factor of 5 larger than the longest axial dimension of neutrophils. However, other analyses suggest the appearance of spatial organization within cellular dimensions (e.g., [14]). Hess and Mikhailov [15] have reported that pattern elements must be >1 μm in size to avoid diffusional mixing; our observed size of 3 to 4 μm is in agreement with the anticipated minimal size. The shape of the pattern elements, stripes, has been described in physical systems [1]. In contrast, spiral Ca^{2+} waves have been observed in large cells such as oocytes [25]. Thus, experimental verification of sustained intracellular metabolic patterns has been achieved.

Our experimental findings coupled with the growing interest in nonlinear systems should stimulate further theoretical work. The fixed boundary concentrations often assumed to address the problem are not evident in the micrographs reported. Indeed, we predict that the time-dependent changes in metabolite concentration and pH in the juxtamembrane region will be an important biological feature of metabolic waves. Changes in metabolite concentrations and pH have been proposed as signaling agents within cells (e.g., [22]). Some analyses rely upon modeling the activity of one glycolytic enzyme, phosphofructokinase. However, glycolytic regulation is complicated and its interactive reaction dynamics remain poorly understood [26].

Cellular dissipative structures may be of biological importance. We have proposed that temporal oscillations in metabolite concentrations play a crucial role in transmembrane signaling [21,22]. Indeed, certain diseases have been linked with defects in neutrophil motility and intracellular NAD(P)H oscillations; these disorders can be ameliorated by perturbing intracellular oscillators into a sinusoidal waveform [27,28]. Thus, temporal organization is biologically significant. Turing [3] first recognized the possibility that reaction-diffusion processes and their nonlinear coupling could give rise to biological patterns. Our work supports this concept and indicates that such patterns are not restricted to the supracellular level. The biological significance of the observed patterns is suggested by the facts that they were unidirectional and observed only in morphologically polarized cells. Physical studies of chemical pattern formation are occasionally justified by

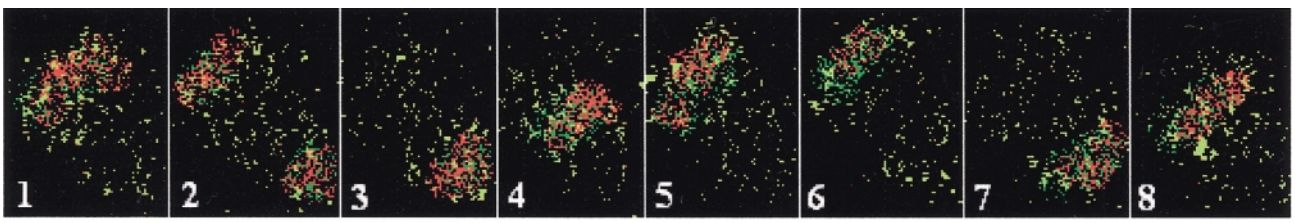

FIG. 3 (color). Images of traveling pH waves in a neutrophil. A time sequence of eight images of a SNARF-1-labeled cell is shown. The lamellipodium is oriented toward the upper left hand side of each frame. Images were collected for 10 msec with a 90 msec interval between micrographs. Of the images collected, only every fifth image is shown for clarity. SNARF-1 fluorescence varies spatially, thus forming a traveling pH wave. The time covered by these images is 4 sec. Data are representative of those obtained on three independent experiments ($\times$1050).

appealing to their biological significance, which now seems appropriate. The wave patterns originate from the uropod. Although the identity of the pacemaker is unknown, a specific locus for calcium waves has been suggested in another cell type; these waves were apparently not driven by diffusion [29]. Our study was limited to NAD(P)H and proton concentrations; however, other conjugate metabolites such as adenosine 5′-triphosphate (ATP) may form self-organized patterns under these conditions. The wave size and velocity suggest that enzymes requiring metabolic products may switch between on and off states. We suggest that dissipative structures may represent a form of information processing and distribution in living cells.

This work was supported by NIH Grant No. CA74120.

*To whom correspondence should be addressed.
Electronic address: hpetty@biology.biosci.wayne.edu

[1] D. Walgraef, *Spatio-Temporal Pattern Formation* (Springer, New York, 1997).
[2] G. Nicolis and I. Prigogine, *Exploring Complexity* (W. H. Freeman & Co., New York, 1989).
[3] A. M. Turing, Philos. Trans. R. Soc. London B **327**, 37 (1952).
[4] V. Castets *et al.*, Phys. Rev. Lett. **64**, 2953 (1990).
[5] Q. Ouyang and H. L. Swinney, Nature (London) **352**, 610 (1991).
[6] A. Goldbeter, *Biochemical Oscillations and Cellular Rhythms* (Cambridge University Press, Cambridge, UK, 1996).
[7] A. N. Zaikin and A. M. Zhabotinskii, Nature (London) **225**, 535 (1970).
[8] J. J. Tyson and J. P. Keener, Physica (Amsterdam) **32D**, 317 (1988).
[9] Z. Noszticzius *et al.*, Nature (London) **329**, 619 (1987).
[10] P. Marmillot, J.-F. Hervagault, and G. R. Welch, Proc. Natl. Acad. Sci. U.S.A. **89**, 12 103 (1992).
[11] A. Goldbeter, Proc. Natl. Acad. Sci. U.S.A. **70**, 3255 (1973).
[12] A. Goldbeter and R. Lefever, Biophys. J. **12**, 1302 (1972).
[13] M. Herschkowitz-Kaufman and G. Nicolis, J. Chem. Phys. **56**, 1890 (1972).
[14] B. Hasslacher, R. Kapral, and A. Lawniczak, Chaos **3**, 7 (1993).
[15] B. Hess and A. Mikhailov, Ber. Bunsen-Ges. Phys. Chem. **98**, 1198 (1994).
[16] T. Mair and S. C. Muller, J. Biol. Chem. **271**, 627 (1996).
[17] S. C. Muller, T. Mair, and O. Steinbock, Biophys. Chem. **72**, 37 (1998).
[18] T. Shinjyo, Y. Nakagawa, and T. Ueda, Physica (Amsterdam) **84D**, 212 (1995).
[19] A. Boiteux and B. Hess, Ber. Bunsen-Ges. Phys. Chem. **84**, 392 (1980).
[20] D. Roos and A. J. M. Balm, *The Reticuloendothelial System: A Comprehensive Treatise*, edited by A. J. Sbarra and R. R. Strauss (Plenum Press, New York, 1980).
[21] H. R. Petty, *Self-Organized Biological Dynamics and Nonlinear Control by External Stimuli*, edited by J. Walleczek (Cambridge University Press, Cambridge, UK, 2000).
[22] A. L. Kindzelskii *et al.*, Biophys. J. **73**, 1777 (1997).
[23] B. Hess and A. Boiteux, Annu. Rev. Biochem. **40**, 237 (1971).
[24] B. Liang and H. R. Petty, J. Cell. Physiol. **152**, 145 (1992).
[25] J. Lechleiter *et al.*, Science **252**, 123 (1991).
[26] A. Arkin, P. Shen, and J. Ross, Science **277**, 1275 (1997).
[27] Y. Adachi *et al.*, J. Invest. Dermatol. **111**, 259 (1998).
[28] S. Shaya *et al.*, J. Invest. Dermatol. **111**, 154 (1998).
[29] T. A. Rooney, E. J. Sass, and A. P. Thomas, J. Biol. Chem. **265**, 10 792 (1990).